The formulation of quantum statistical mechanics based on the Feynman path centroid density. I. Equilibrium properties

Jianshu Cao and Gregory A. Voth
Department of Chemistry, University of Pennsylvania, Philadelphia, Pennsylvania 19104-6323

(Received 28 October 1993; accepted 16 December 1993)

A formulation of quantum statistical mechanics is discussed in which the Feynman path centroid density in Feynman path integration is recast as the central statistical distribution used to average equilibrium and dynamical quantities. In this formulation, the path integral centroid density occupies the same role as the Boltzmann density in classical statistical mechanics. Therefore, the statistical ensemble of imaginary time path centroid configurations provides the distribution which is used to average the appropriately formulated effective operators and imaginary time correlation functions. An accurate renormalized diagrammatic perturbation theory for the centroid density and centroid-constrained imaginary time propagator will also be described with particular emphasis given to the mathematical advantages arising from the centroid-based formulation. The present paper is concerned with the calculation of equilibrium properties from the centroid perspective, while the companion paper describes a centroid-based formalism for calculating dynamical time correlation functions.

I. INTRODUCTION

The Feynman path integral representation of quantum mechanics,[1] and in particular the representation of quantum statistical mechanics,[2,3] provides a powerful method to calculate and visualize natural processes. For example, path integrals are particularly useful in describing the quantum mechanics of an equilibrium system because the canonical distribution for a single quantum particle in the path integral picture becomes isomorphic with that for a classical "ring polymer" of quasiparticles[3,4] (cf. Fig. 1). In the discretized path integral representation, the partition function for a quantum particle is given by the expression[3,4]

$$Z=\lim_{P\to\infty}\left(\frac{mP}{2\pi\hbar^2\beta}\right)^{P/2}\int dq_1\cdots\int dq_P\,\exp[-\beta V_P(\mathbf{q})], \tag{1.1}$$

where m is the particle mass, β equals $1/k_BT$, and the isomorphic quasiclassical polymer potential V_P is given by

$$V_P(\mathbf{q})=\sum_{i=1}^{P}\left[\frac{mP}{2\hbar^2\beta^2}\,(q_i-q_{i+1})^2+\frac{V(q_i)}{P}\right]. \tag{1.2}$$

In this discrete representation, the coordinates $\{q_i\}$ describe the positions of the classical quasiparticles and have the cyclic property such that $q_{i+P}=q_i$ (cf. Fig. 1). Each quasiparticle is harmonically bound to its two nearest neighbors and it "feels" the interaction potential through the term $V(q_i)/P$. In numerical applications, a finite value of the discretization parameter P is used which is large enough so that suitable numerical convergence is obtained.[3] While the above equations have been written for a single quantum particle in one dimension, a generalization to multiple particles and/or dimensions is straightforward.[1-4] In the discretized representation, the path integral formalism has allowed for the numerical simulation of highly nontrivial quantum systems using path integral Monte Carlo (PIMC) or molecular dynamics techniques.[3]

In the fully quantum ($P\to\infty$) limit, the path integral for, e.g., the partition function is expressed as a functional integral over all possible paths $q(\tau)$ such that[2]

$$Z=\int\cdots\int \mathscr{D}(\tau)\exp\{-S[q(\tau)]/\hbar\}, \tag{1.3}$$

where the exponential weighting of the paths is determined by the imaginary time action functional[2]

$$S[q(\tau)]=\int_0^{\hbar\beta} d\tau\left\{\frac{m}{2}\,\dot{q}(\tau)^2+V[q(\tau)]\right\}. \tag{1.4}$$

Analytically, the path integral method has proven to be particularly advantageous in the theoretical analysis of several condensed matter problems such as the polaron[5] and the solvated electron.[6]

One of the many interesting ideas suggested by Feynman in his formulation and application of path integrals is the notion of the path centroid variable,[7] denoted here by the symbol q_0. The centroid is the imaginary time average of a particular closed Feynman path $q(\tau)$ which, in turn, is simply the zero-frequency Fourier mode of that path, i.e.,

$$q_0=\frac{1}{\hbar\beta}\int_0^{\hbar\beta} d\tau\, q(\tau). \tag{1.5}$$

In the discretized path integral picture (i.e., for finite P), the path centroid variable is equivalent to the center of mass of the isomorphic polymer of classical quasiparticles (cf. Fig. 1) such that

$$q_0=\frac{1}{P}\sum_{i=1}^{P} q_i. \tag{1.6}$$

(It should be noted that in some previous publications, the centroid variable has been denoted by $\bar{q}_0$ rather than q_0. The tilde notation will be reserved in the present paper for another use.)

 0021-9606/94/100(7)/5093/13/$6.00

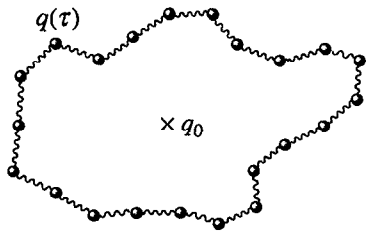

FIG. 1. A schematic diagram depicting a discretized Feynman path $q(\tau)$ within the imaginary time interval $0 \leq \tau \leq \hbar\beta$. The isomorphic classical quasiparticles are shown by the dark circles which form a "ring polymer." Each quasiparticle "interacts" with its two nearest neighbors through effective harmonic forces and feels the external potential through the term $V(q_i)/P$ [cf. Eq. (1.2)]. The centroid variable q_0 defined in Eqs. (1.5) and (1.6) is also shown.

Feynman noted that a quantum mechanical "centroid density" $\rho_c(q_c)$ can be defined for the path centroid variable which is the path sum over all paths with their centroids located at some point in space denoted by q_c. Specifically, the formal expression for the centroid density is given by

$$\rho_c(q_c)=\int \cdots \int \mathscr{D}q(\tau)\,\delta(q_c-q_0)\exp\{-S[q(\tau)]/\hbar\}. \quad (1.7)$$

The quantum partition function in Eq. (1.3) is then obtained by the integration of the centroid density over all possible positions of the centroid, i.e.,

$$Z=\int dq_c\, \rho_c(q_c). \quad (1.8)$$

Some caution is in order when one uses the centroid density because it is distinctly different from the coordinate (or particle) density $\rho(q)$ given by

$$\rho(q)=\langle q|e^{-\beta H}|q\rangle=\int \cdots \int \mathscr{D}q(\tau)\,\delta[q-q(0)] \times \exp\{-S[q(\tau)]/\hbar\}, \quad (1.9)$$

where $q(0)$ is the beginning and end point of the cyclic quantum path $q(\tau)$ and is *definitely not* the centroid variable in Eq. (1.5). Thus, the particle density function is the diagonal element of equilibrium density matrix in the coordinate representation, while the centroid density does not have a similar physical interpretation. Nevertheless, the integration over either density yields the quantum partition function.

Feynman used the definition of the centroid density along with a simple approximation for the action functional in Eq. (1.4) to derive an expression for a quasiclassical partition function.[7] The latter function is expressed as an integration over an effective Boltzmann factor which, in turn, depends on a variational effective potential determined at each value of the centroid variable with the help of an appropriate centroid density formulation[8] of the Gibbs–Bogoliubov variational principle. In subsequent work, several authors[9–11] have improved on Feynman's original approach by using a more physically accurate variational harmonic reference system to describe the imaginary time path fluctuations around the centroid variable. The effective harmonic frequency and effective potential are again determined at each value of the centroid variable, resulting in an approximate expression for the centroid density in Eq. (1.7). An approximate variational partition function[9–11] can then be determined in such a theory by virtue of Eq. (1.8).

One conclusion that can be reached from the aforementioned work of Feynman[7] and others,[9–11] as well as from the apparent utility of the centroid density-based formulation of quantum transition state theory,[12] is that the centroid density is a particularly useful quantity about which to develop approximate, but highly accurate, quantum mechanical expressions and to probe the quantum-classical correspondence principle in statistical mechanics. It is in this spirit that a more general centroid density-based formulation of quantum Boltzmann statistical mechanics is presented in the present paper. This formulation is based on a single important notion: In any such theory, the centroid density should occupy the same role as the Boltzmann density in classical statistical mechanics. That is, the rules for calculating operator averages and imaginary time correlation functions should be reformulated so that the final result of such a calculation is obtained by an integration over the centroid density (i.e., by a statistical weighting with the centroid density). It will be shown that such a formulation is not completely trivial due to the mathematical differences between the centroid approach and the usual rules of quantum statistical mechanics. Nevertheless, the resulting expressions are quite interesting both in terms of the classical-quantum correspondence principle and from the analytical point of view. One result from this approach is that the centroid formulation seems to actually simplify the calculation of some quantum mechanical quantities since the imaginary time path fluctuations have been "preaveraged" in the centroid density expression. This statement is particularly true in the case of quantum *dynamics* (i.e., time correlation functions) which are discussed in the companion paper[13] and in Ref. 14.

Another significant feature of the centroid density-based formulation of statistical mechanics is that by concentrating on the centroid density as the central statistical distribution, a formally exact diagrammatic expansion for the centroid density can be employed which turns out to be simplified from the point of view of the relevant diagram topologies. The diagrammatic expansion is also particularly amenable to powerful renormalization techniques. The diagrammatic theory draws the formal connection between various variational expressions for the centroid density which have been derived by others[9–11] and specific diagram resummation and renormalization strategies. A systematic approach to improve on the result of the variational centroid density theory thus emerges. A considerable amount of time will be devoted to the diagrammatic methods in the present article due to the central practical and formal importance of the centroid density in the formalism.

The sections of this paper are organized as follows: In Sec. II, the basic equations are derived for operator averages and imaginary time correlation functions in the centroid density-based formulation of quantum statistical mechanics. The diagrammatic methods for the centroid density and related quantities are then discussed in Sec. III, while applica-

tions are presented in Sec. IV. Concluding remarks are given in Sec. V.

II. GENERAL FORMALISM

In this section, the general formulation of quantum Boltzmann statistical mechanics in terms of the centroid density is discussed. The term "general formulation" means that the rules are presented here with which to calculate operator averages and imaginary time correlation functions in the centroid density perspective at different levels of approximation. The emphasis in this section will not be on new numerical procedures which might or might not have advantages over the already well-established and successful numerical path integral techniques (see, e.g., Ref. 3). Rather, the theoretical development is more of a conceptual one which is intended to explore the quantum-classical correspondence in statistical mechanics. Moreover, the rules outlined below for calculating averages and correlation functions are formulated on the assumption that a good analytic expression for the centroid density can be obtained (cf. Sec. III), thereby bypassing the need for a fully numerical approach. Future research will be devoted to an exploration of any numerical advantages inherent in the centroid-based imaginary time path integral formulation. In the companion paper,[13] it will indeed be shown that the centroid-based approach provides a quite promising computational approach for the determination of quantum real time correlation functions.[14]

A. Imaginary time position correlation functions

At this point, it is advantageous to introduce the notion of a centroid-constrained imaginary time propagator, i.e., the correlation function of quantum path fluctuations with respect to the position of the centroid variable $q_0=q_c$. This correlation function is defined as

$$C_c(\tau,q_c)=\frac{\int\cdots\int \mathscr{D}q(\tau)\,\delta(q_c-q_0)[q(\tau)-q_0][q(0)-q_0]\exp\{-S[q(\tau)]/\hbar\}}{\int\cdots\int \mathscr{D}q(\tau)\,\delta(q_c-q_0)\exp\{-S[q(\tau)]/\hbar\}}. \tag{2.1}$$

As the centroids of the paths $q(\tau)$ in this correlation function are constrained to be at q_c, the paths can be rewritten as $q(\tau)=q_c+\tilde{q}(\tau)$, where $\tilde{q}(\tau)$ is the quantum path fluctuation with respect to the centroid. A Fourier decomposition of the paths $\tilde{q}(\tau)$ can now be introduced such that

$$\tilde{q}(\tau)=\sum_{n\neq 0}\hat{q}_n e^{-i\Omega_n\tau}, \tag{2.2}$$

where the summation is over all positive and negative integers except for $n=0$, and Ω_n is the Euclidean frequency defined by $\Omega_n=2\pi n/\hbar\beta$.

The correlation function in Eq. (2.1) differs from the usual Euclidean position correlation function $C(\tau)$ because only the paths with centroids at q_c contribute to the centroid-constrained propagator $C_c(\tau,q_c)$. However, one can obtain $C(\tau)$ by averaging the centroid-constrained propagator over the normalized centroid density $\rho_c(q_c)/Z$, i.e.,

$$C(\tau)=\langle q(\tau)q(0)\rangle=\langle C_c(\tau,q_c)+q_c^2\rangle_{\rho_c}, \tag{2.3}$$

or, equivalently,

$$\tfrac{1}{2}\langle|q(\tau)-q(0)|^2\rangle=C(0)-C(\tau)$$
$$=\langle C_c(0,q_c)\rangle_{\rho_c}-\langle C_c(\tau,q_c)\rangle_{\rho_c}. \tag{2.4}$$

It should be noted that the imaginary time function in Eq. (2.4) provides a measure of the localization of quantum particles in condensed media.[3,4,6] From this point onward, the notation $\langle\cdots\rangle_{\rho_c}$ denotes an averaging by integrating some centroid-dependent function over the centroid position q_c weighted by the normalized centroid density $\rho_c(q_c)/Z$.

A general method to obtain the correlation function $C_c(\tau,q_c)$ is through functional differentiation of a generating functional. In order to formulate such a functional, an imaginary time-dependent force $f(\tau)$ is introduced into the action functional of the centroid density [Eq. (1.7)] such that the potential $V[q(\tau)]$ is replaced by $V[q(\tau)]+f(\tau)\tilde{q}(\tau)$. The centroid-constrained propagator is then given by

$$C_c(\tau,q_c)=\lim_{f\to 0}\frac{1}{\rho_c}\frac{\delta^2\rho_c[f(\tau)]}{\delta f(\tau)\,\delta f(0)}. \tag{2.5}$$

Here, the centroid density ρ_c is understood to be a functional of the extra time-dependent force $f(\tau)$ and is therefore the generating functional[15] for the centroid-constrained correlation function.

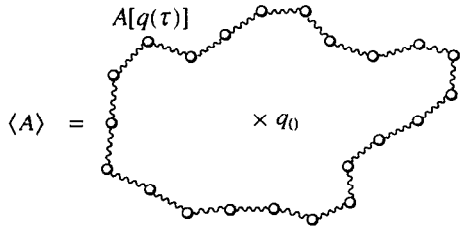

FIG. 2. A schematic diagram depicting the calculation of an operator average $\langle A\rangle$ in the discretized Feynman path integral picture. The operator $A[q(\tau)]$ can be evaluated anywhere on the path integral ring $0\leq\tau\leq\hbar\beta$ due to the cyclic invariance of the trace operation. The centroid variable, which is off the ring, is also shown.

B. Operator averages

In the normal path integral perspective,[2,3] the canonical average of an operator A is given by the expression

$$\langle A\rangle = Z^{-1}\int \cdots \int \mathscr{D}q(\tau) A[q(0)] \exp\{-S[q(\tau)]/\hbar\}, \quad (2.6)$$

Due to the cyclic invariance of the trace, the operator can be evaluated at any point along the cyclic imaginary time path $q(\tau)$. This situation is depicted in Fig. 2 where the centroid variable, which is off the ring, is also shown. The challenge therefore is to reformulate the rules for calculating the operator average, so that the centroid density can be used in the statistical averaging.[11] In order to do this, the average in Eq. (2.6) is first re-expressed as

$$\langle A\rangle = \int dq_c \left(\frac{\int \cdots \int \mathscr{D}q(\tau)\, \delta(q_c - q_0) A[q(\tau)] \exp\{-S[q(\tau)]/\hbar\}}{\int dq_c\, \rho_c(q_c)} \right). \quad (2.7)$$

The operator A is then represented in Fourier space, i.e.,

$$A(q) = \int \frac{dk}{2\pi}\, \hat{A}(k) e^{ikq}, \quad (2.8)$$

where $\hat{A}(k)$ is the Fourier transform of the operator. Equation (2.6) can then be written as

$$\langle A\rangle = Z^{-1}\int dq_c\, \rho_c(q_c) \int \frac{dk}{2\pi}\, \hat{A}(k) e^{ikq_c} \left(\frac{\int \cdots \int \mathscr{D}\tilde{q}(\tau) e^{ik\tilde{q}(\tau)} \exp\{-S[q_c+\tilde{q}(\tau)]/\hbar\}}{\int \cdots \int \mathscr{D}\tilde{q}(\tau) \exp\{-S[q_c+\tilde{q}(\tau)]/\hbar\}} \right), \quad (2.9)$$

where the notation for the action functional "$S[q_c+\tilde{q}(\tau)]$" is understood to denote path fluctuations around a fixed centroid at q_c. At this point, a cumulant average of the term $\exp[ik\tilde{q}(\tau)]$ in the brackets in Eq. (2.9) can be performed over the path fluctuation variable $\tilde{q}(\tau)$. This average, for the present purposes, is truncated at second order, but it need not be. [The variable $\tilde{q}(\tau)$ is also assumed to have symmetric fluctuations about the centroid.] After performing the inverse Fourier transformation by integrating over k in Eq. (2.7), one arrives at the final result of the analysis which is given by

$$\langle A\rangle = \langle A_c(q_c)\rangle_{\rho_c}, \quad (2.10)$$

where the effective centroid-dependent quasiclassical function A_c is given by

$$A_c(q_c) = \langle A(q_c+\tilde{q})\rangle_{C_c(0,q_c)} = \frac{1}{\sqrt{2\pi C_c(0,q_c)}} \int d\tilde{q}\, A(q_c+\tilde{q}) \times \exp[-\tilde{q}^2/2C_c(0,q_c)]. \quad (2.11)$$

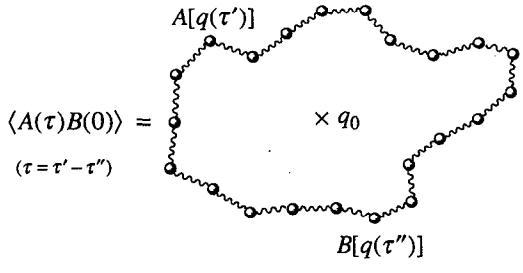

FIG. 3. A schematic diagram depicting the calculation of the imaginary time correlation function $\langle A(\tau)B(0)\rangle$ in the discretized Feynman path integral picture. The operators $A[q(\tau')]$ and $B[q(\tau'')]$ can be evaluated at any two points on the path integral ring subject to the constraint $0 \leq \tau = \tau' - \tau'' \leq \hbar\beta$. The centroid variable, which is off the ring, is also shown.

Here, the variable $\tilde{q}$ is obviously a Gaussian variable with a width factor $C_c(0,q_c)$. The effective classical function $A_c(q_c)$ depends on the centroid variable q_c and, in order to calculate the canonical average $\langle A\rangle$, is averaged in a classical-like fashion in Eq. (2.10) with the normalized centroid density $\rho_c(q_c)/Z$. The above result has been obtained previously by one of us[11] from the somewhat more specialized perspective of the Feynmann–Hibbs theory.[7] If one has an analytic or numerical representation of the centroid density $\rho_c(q_c)$, a numerical quadrature strategy can be employed for evaluating Eq. (2.10) for cases in which the integral in Eq. (2.11) cannot be solved analytically. For multidimensional systems, a better numerical strategy might be to use a Monte Carlo procedure in which Eqs. (2.10) and (2.11) are combined in a single MC calculation based on the importance sampling function $W(\tilde{q},q_c) = \rho_c(q_c) \times \exp[-\tilde{q}^2/2C_c(0,q_c)]$, assuming again that an analytical expression for $C_c(0,q_c)$ has been obtained (cf. Sec. III C below).

It should be noted that the effective centroid-based representation of the operator A in Eq. (2.11), while useful in the context of the equilibrium averages, also occupies a central role in a semiclassical algorithm to calculate quantum time correlation functions in the centroid perspective.[13]

C. General imaginary time correlation functions

A general imaginary time correlation function for coordinate-dependent operators is defined as[3]

$$C_{AB}(\tau) = \langle A[q(\tau)] B[q(0)]\rangle = Z^{-1}\int \cdots \int \mathscr{D}q(\tau) A[q(\tau)] B[q(0)] \times \exp\{-S[q(\tau)]/\hbar\}, \quad (2.12)$$

where the operators $A[q(\tau)]$ and $B[q(0)]$ can be evaluated

anywhere along the path such that $0 \leq \tau \leq \hbar\beta$. This situation is depicted in Fig. 3 and, again, the challenge is to reformulate these rules so that the centroid density, which is off the ring, can be utilized. In order to do this, one can use the fact that the correlation function $C_{AB}(\tau)$ can always be expressed in terms of the centroid-constrained propagator $C_c(\tau,q_c)$ in Eq. (2.1) at the level of a second-order cumulant approximation. To proceed, one first rewrites Eq. (2.12) as

$$C_{AB}(\tau)=\int dq_c \left\{ \frac{\int\cdots\int \mathcal{D}q(\tau)\delta(q_c-q_0)A[q(\tau)]B[q(0)]\exp[-S[q(\tau)]/\hbar]}{\int dq_c\, \rho_c(q_c)} \right\}. \tag{2.13}$$

The operators A and B are next written in Fourier space as in Eq. (2.8). Then, Eq. (2.12) becomes

$$C_{AB}(\tau)=Z^{-1}\int dq_c\, \rho_c(q_c)\int \frac{dk_1}{2\pi}\int \frac{dk_2}{2\pi}\, \hat{A}(k_1)\hat{B}(k_2)\exp[i(k_1+k_2)q_c] \times\left[\frac{\int\cdots\int \mathcal{D}\tilde{q}(\tau)\exp\{i[k_1\tilde{q}(\tau)+k_2\tilde{q}(0)]\}\exp\{-S[q_c+\tilde{q}(\tau)]/\hbar\}}{\int\cdots\int \mathcal{D}\tilde{q}(\tau)\exp\{-S[q_c+\tilde{q}(\tau)]/\hbar\}} \right], \tag{2.14}$$

The centroid-constrained average in the bracket can be performed as a cumulant expansion which, for the present purpose, is truncated at second order. The result for the bracketed term is then given by

$$\langle \exp[ik_1\tilde{q}(\tau)+ik_2\tilde{q}(0)]\rangle_c \simeq \exp\left\{ -\frac{1}{2}\,[k_1^2C_c(0,q_c)+2k_1k_2C_c(\tau,q_c)+k_2^2C_c(0,q_c)] \right\}. \tag{2.15}$$

In order to perform the integrals over k_1 and k_2 in Eq. (2.14), a coordinate rotation is first performed such that

$$q_+(\tau)=[q(\tau)+q(0)]/\sqrt{2},$$
$$q_-(\tau)=[q(\tau)-q(0)]/\sqrt{2}, \tag{2.16}$$

and new centroid-constrained position correlation functions are defined as

$$C_c^+(\tau,q_c)=C_c(0,q_c)+C_c(\tau,q_c),$$
$$C_c^-(\tau,q_c)=C_c(0,q_c)-C_c(\tau,q_c). \tag{2.17}$$

After performing the integrals in Fourier space, one arrives at the final result for the imaginary time correlation function in the centroid density picture

$$C_{AB}(\tau)=\langle \mathcal{A}_{AB}(\tau,q_c)\rangle_{\rho_c}, \tag{2.18}$$

where the centroid-dependent imaginary time-correlated operator product $\mathcal{A}_{AB}(\tau,q_c)$ is defined in the centroid density picture by the double-Gaussian average

$$\mathcal{A}_{AB}(\tau,q_c)=\langle A[q_c+2^{-1/2}(q_++q_-)]B[q_c+2^{-1/2}(q_+-q_-)]\rangle_{C_c^+,C_c^-}. \tag{2.19}$$

Here, q_+ and q_- are Gaussian variables with width factors $C_c^+(\tau,q_c)$ and $C_c^-(\tau,q_c)$, respectively.

The double Gaussian average form for the centroid-constrained operator product in Eq. (2.19) is somewhat complicated to implement, particularly if the operators A or B are not polynomials or exponentials in the variable q. It should also be noted that if the cumulant expansion is carried out beyond quadratic order in Eq. (2.15), an even more complicated analytical form of Eq. (2.19) would be obtained. However, it is also important to remember that in an analytical calculation of the imaginary time correlation function $C_{AB}(\tau)$ in the conventional path integral formalism, both the diagonal *and* off-diagonal elements of the thermal density matrix are required. The formalism embodied in Eq. (2.18) requires only an accurate value of the centroid density $\rho_c(q_c)$ and the centroid-constrained representation of the correlated operator product in Eq. (2.19), albeit the latter expression is somewhat complicated. As in the case of operator averages (Sec. II B), a numerical quadrature procedure can be employed if Eq. (2.19) cannot be evaluated analytically. In the case of multidimensional systems, a combined Monte Carlo procedure for evaluating Eq. (2.18) simultaneously with Eq. (2.19) can be developed using importance sampling based on the centroid density and the double-Gaussian distribution in Eqs. (2.18) and (2.19), respectively, if $C_c(0,q_c)$ is also known analytically.

III. DIAGRAMMATIC THEORY

A. Exact diagrammatic representation of the centroid density

Because of its central importance in the centroid-based theory, a systematic study is presented in this section of the perturbation expansion, or equivalently, the exact cumulant expansion of the centroid density. This expansion has a one-to-one correspondence with a diagrammatic representation. It will be shown that diagrammatic classifications and topological reductions result in the renormalization of the vertices and lines, and thus lead to a set of self-consistent equations. Previous results based on an optimized harmonic reference potential[9–11] can be readily derived and thus systematically improved. Furthermore, the small parameter in the present theory is $\hbar^2$, so the underlying classical limit of the theory is the *exact* classical equilibrium density function for any given system.

In general, it will be assumed that the Euclidean action

of the reference system takes a quadratic form in the path fluctuations variable $\tilde{q}(\tau)$ such that

$$S_{\rm ref}[\tilde{q}(\tau)]=\int_0^{\hbar\beta} d\tau\left\{\frac{m}{2}\,\dot{\tilde{q}}(\tau)^2+V_{\rm ref}[\tilde{q}(\tau)]\right\}$$
$$=\sum_{n=-\infty}^{\infty}\frac{|\hat{q}_n|^2}{2\alpha_n}, \tag{3.1}$$

where α_n defines the reference centroid-constrained propagator [cf. Eq. (2.1)] such that

$$\alpha(\tau)=\sum_{n\neq 0}\alpha_n e^{-i\Omega_n\tau}, \tag{3.2}$$

and $\alpha_0=0$ due to the centroid constraint. Two well-known quadratic models are the free-particle reference system, where $\alpha_n^{-1}=m\beta\Omega_n^2$, and the linear harmonic oscillator (LHO) reference system, where $\alpha_n^{-1}=m\beta(\Omega_n^2+\omega^2)$, with ω being the intrinsic LHO frequency.

With a solvable reference system in hand, one can express the centroid density as

$$\rho_c(q_c)=\rho_{c,\rm ref}(q_c)\langle\exp(-\beta\overline{\Delta V})\rangle_{c,\rm ref}, \tag{3.3}$$

where $\overline{\Delta V}$ is the imaginary time average

$$\overline{\Delta V}=\frac{1}{\hbar\beta}\int_0^{\hbar\beta} d\tau\,\Delta V[q_c+\tilde{q}(\tau)] \tag{3.4}$$

and $\Delta V=V-V_{\rm ref}$ is the deviation of the real potential V from the reference potential $V_{\rm ref}$. The symbol $\langle\cdots\rangle_{c,\rm ref}$ in Eq. (3.3) denotes a centroid-constrained path integral average in the reference system. As the centroid-constrained propagator of the reference potential $\alpha(\tau)$ uniquely defines an infinite set of Gaussian averages over the Fourier modes $\{\hat{q}_n\}$, one can equivalently denote the centroid-constrained average in the reference system with the symbol $\langle\cdots\rangle_\alpha$.

The first step in the development of a diagrammatic theory for the centroid density is to Taylor expand the average in Eq. (3.3), i.e.,

$$\langle\exp(-\beta\overline{\Delta V})\rangle_\alpha$$
$$=\sum_0^{\infty}\frac{1}{n!}\left\langle\left\{-\frac{1}{\hbar}\int_0^{\hbar\beta} d\tau\,\Delta V[q_c+\tilde{q}(\tau)]\right\}^n\right\rangle_\alpha$$
$$=\sum_{n=0}^{\infty}\frac{1}{n!}\left\langle\left[-\frac{1}{\hbar}\int_0^{\hbar\beta} d\tau\int\frac{dk}{2\pi}\right.\right.$$
$$\left.\left.\times\Delta\hat{V}(k,q_c)e^{ik\tilde{q}(\tau)}\right]^n\right\rangle_\alpha, \tag{3.5}$$

where $\Delta\hat{V}(k,q_c)$ is the spatial Fourier transformation of difference potential $\Delta V(q_c+\tilde{q})$ with respect to the variable $\tilde{q}$. It should be noted that the subscript n in Eq. (3.5) differs from that used in the Fourier expansion in Eq. (3.2). Since $\tilde{q}(\tau_i)$ in the reference system is a Gaussian variable with zero mean at any imaginary time τ_i, the cumulant expansion of a linear combination of those variables truncates at second order, giving

$$\left\langle\prod_{i=1}^{n} e^{ik_i\tilde{q}(\tau_i)}\right\rangle_\alpha$$
$$=\exp\left\{-\left[\frac{1}{2}\sum_{i=1}^{n}k_i^2\alpha(0)+\frac{1}{2}\sum_{i\neq j}^{n}k_ik_j\alpha(\tau_i-\tau_j)\right]\right\}, \tag{3.6}$$

in which $\alpha(\tau)$ is defined by Eq. (3.2). There is no linear term in Eq. (3.6) because $\langle\tilde{q}\rangle=0$ according to the definition of the variable $\tilde{q}(\tau)$ being the path fluctuation with respect to the centroid. This property greatly simplifies the cumulant expansion and diagrammatic analysis. By substituting the Taylor expansion of Eq. (3.6) into Eq. (3.5), and transforming back into coordinate space, one arrives at the result

$$\langle\exp(-\beta\overline{\Delta V})\rangle_{\rm ref}^{c}=\sum_{n=0}^{\infty}\sum_{m=0}^{\infty}\frac{(-1)^n}{n!m!}$$
$$\times\prod_{i'=1}^{n}\int_0^{\hbar\beta}\frac{d\tau_{i'}}{\hbar}\left[\frac{1}{2}\sum_{i=1}^{n}\alpha(0)\partial_i^2\right.$$
$$\left.+\frac{1}{2}\sum_{i\neq j}^{n}\alpha(\tau_i-\tau_j)\partial_i\partial_j\right]^m\Delta\mathbf{V}, \tag{3.7a}$$

where

$$\Delta\mathbf{V}\equiv\prod_{l=1}^{n}\Delta V[q_c+\tilde{q}(\tau_l)]|_{\tilde{q}=0} \tag{3.7b}$$

and the partial derivative symbol is defined to be $\partial_i\equiv\partial/\partial\tilde{q}(\tau_i)$ applied at time slice τ_i. The imaginary time integrals in Eq. (3.7a) are understood to be integrations over any and all imaginary time slices which appear in the expansion. After the derivatives are taken, the potential difference terms are evaluated at the position of the centroid q_c.

In principle, the above perturbation series gives a complete description of the quantum mechanical centoid density and the expansion can be carried out to any order according to the accuracy required for a specific problem. However, it is conceivable that, in higher orders, the expansion terms become increasingly complicated and a low-order calculation will not provide a reasonable physical picture of a quantum system. Therefore, a diagrammatic representation of Eq. (3.7) is introduced here which provides a powerful way to analyze the perturbation expression and to visualize the analytical expressions.

A careful examination of the series in Eq. (3.7) reveals the basic composition of the expansion terms. That is, all diagrams consist of two basic elements, vertices and lines. Each vertex is designated by a Euclidean time τ_i to be integrated from $\tau_i=0$ to $\tau_i=\hbar\beta$, and the potential, or its derivatives, are evaluated at the position of the centroid. Each line connecting two vertices at times τ_i and τ_j is designated as a reference centroid-constrained propagator $\alpha(\tau_i-\tau_j)$. Whenever a line connects to a vertex, a spatial derivative is applied to the potential so that the order of the derivative is equal to the number of lines that connect to the vertex. A negative

sign is assigned to each vertex. The value of a diagram is the product of all the composing elements which multiply a symmetry coefficient determined by the topological structure of the diagram.

With above definitions in hand, one can establish a one-to-one correspondence between each distinct perturbation term and each diagram. The expansion series of Eq. (3.7) is then the collection of all topologically different diagrams and all possible combinations. The following diagrams are some examples:

$\langle \exp(-\beta\overline{\Delta V})\rangle_\alpha$

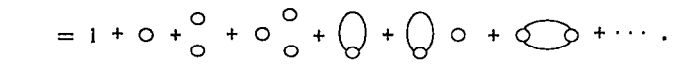

(3.8)

A well-known graph theorem[16] states that an infinite series of all possible topologically different diagrams and their combinations is equal to the exponential of all possible topologically different connected diagrams. For a connected diagram, any two vertices are linked to each other by at least one line or one path of lines. Therefore, one can to express the centroid density as

$$\rho_c(q_c)=\rho_{c,\mathrm{ref}}(q_c)\exp(\mathscr{F}), \tag{3.9}$$

where $\mathscr{F}$ is given by

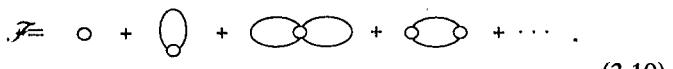

(3.10)

The underlying diagrammatic techniques employed here are not new, having appeared many times in the literature such as in the Meyer cluster expansion[17] and the Feynman diagrams.[18] However, in order to apply these techniques to a specific problem, one must search for the proper diagrammatic representation. In the case of the centroid density, the present approach is not restricted by the functional form of the potential and proves to be particularly advantageous in analytical studies. It should also be noted that the topological reduction performed in the present case is equivalent to a diagrammatic representation of the cumulant expansion. The cumulant expansion itself becomes tedious in high orders and there are a large number of cancellations in the present approach not given explicitly in the cumulant relations. It therefore proves to be much easier to keep track of higher order terms in the diagrammic representation.

As pointed out earlier, all the diagrams of $\mathscr{F}$ are closed due to the fact that $\alpha_0=0$ (i.e., the centroid constraint). For example, there exists no class of diagrams D with single lines hanging outside of the main diagram, such as

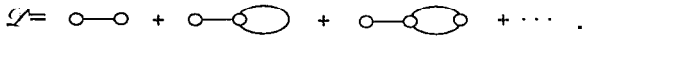

(3.11)

These kinds of diagrams contribute, e.g., to the expansion for the usual quantum density $\langle q|\exp(-\beta H)|q\rangle$. This feature of Eq. (3.10) simplifies the analysis enormously and makes the centroid density perspective a preferable choice for the analytical calculation of equilibrium averages and imaginary time correlation functions in quantum statistical mechanics. It remains to be seen, however, whether the centroid perspective can offer any numerical advantage over standard numerical path integral approaches for calculating equilibrium properties.[3] This issue will be explored in future research.

B. Renormalization of the vertices

The diagrammatic representation of the centroid density enhances our intuition and capability in an approximate evaluation of the full perturbation series. Instead of a tedious term-by-term calculation, one can focus on a class of diagrams with the same topological characteristics. The sum of such a class often results in a compact analytical expression which includes infinite terms in the summation. A very useful technique in such cases is the renormalization of diagrams.[19] This procedure is first applied here to the vertices to obtain an effective potential and thereby an accurate approximation to the centroid density.

The first set of diagrams to be studied contain only one vertex, i.e.,

$$=-\beta\Delta V-\frac{1}{2}\beta\Delta V^{(2)}\alpha(0)-\frac{1}{2^2 2!}\beta\Delta V^{(4)}\alpha^2(0)+\cdots, \tag{3.12}$$

where the superscripts "(i)" denote the order of the spatial derivative and all terms ΔV and $\Delta V^{(i)}$ are evaluated at the centroid position q_c. The different terms in Eq. (3.12) correspond to the corrections due to local quantum path fluctuations $\tilde{q}(\tau)$. Summing up the series, one obtains a closed form expression for Eq. (3.12) in the form of a Gaussian average over a single variable with a Gaussian width factor $\alpha(0)$ such that

$$\langle \Delta V\rangle_\alpha=\frac{1}{\sqrt{2\pi\alpha(0)}}\int d\tilde{q}\ \Delta V(q_c+\tilde{q})\exp[-\tilde{q}^2/2\alpha(0)]. \tag{3.13}$$

This form of the effective potential incorporates to a certain degree quantum effects and the anharmonicity of the potential. In the case of the free particle reference system, the centroid-constrained propagator is given by

$$\alpha_{fp}(\tau)=\frac{\lambda^2}{2}\ [3(1-2u)^2-1], \tag{3.14}$$

where $u=\tau/\hbar\beta$ and $\lambda^2=\hbar^2\beta/12m$. Substitution of this expression for $\alpha(0)$ in Eq. (3.13), and using fact that for the free particle reference system $V_{\mathrm{ref}}=0$, one recovers the well-known Feynman–Hibbs quasiclassical theory[7] for the centroid-dependent effective classical potential from Eq. (3.13). Of course, any general quadratic reference system for the propagator $\alpha(\tau)$ can be used in the present theory and will lead to greater accuracy (see below).

The next order diagram to be considered is a ring diagram with two vertices and two lines, i.e.,

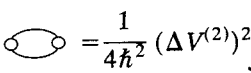

$$=\frac{1}{4\hbar^2}(\Delta V^{(2)})^2\int_0^{\hbar\beta}d\tau_1\int_0^{\hbar\beta}d\tau_2\ \alpha^2(\tau_1-\tau_2). \tag{3.15}$$

As an example, substituting Eq. (3.14) into Eq. (3.15) yields the first correction term to the Feynman–Hibbs approximation

$$\frac{1}{4\hbar^2}(\Delta V^{(2)})^2\int_0^{\hbar\beta}d\tau_1\int_0^{\hbar\beta}d\tau_2\ \alpha_{fp}^2(\tau_1-\tau_2)$$

$$=\frac{\beta^2\lambda^4}{20}(V^{(2)})^2. \tag{3.16}$$

which is exactly what one would expect from the cumulant expansion [see, e.g., Eq. (2.28) in Ref. 10]. Again, any quadratic reference propagator $\alpha(\tau)$ could be used here instead of the free particle one.

A further correction is to add local quantum fluctuations to the diagrams with two vertices, the latter diagrams being given by

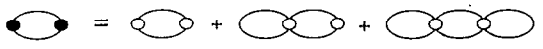

(3.17)

This procedure is equivalent to replacing the potential ΔV in Eq. (3.15) with the effective potential $\langle\Delta V\rangle_\alpha$ of Eq. (3.13). This correction can be introduced in the same fashion for all higher-order diagrams. However, before doing this, it is advantageous to include more diagrams in the vertex corrections. The set of local fluctuation diagrams [Eq. (3.12)] is only the simplest correction. One can extend the analysis to incorporate all ring corrections, given by

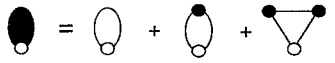

$$=-\frac{1}{2\hbar}\Delta V^{(2)}\int_0^{\hbar\beta}d\tau_1\ \alpha(\tau_1)$$

$$+\frac{1}{2\hbar^2}\Delta V^{(2)}\int_0^{\hbar\beta}d\tau_1\int_0^{\hbar\beta}d\tau_2$$

$$\times\alpha(\tau_1-\tau_2)\alpha(\tau_2-\tau_1)\langle\Delta V^{(2)}\rangle_\alpha+\cdots. \tag{3.18}$$

By expressing the convolution integrals in the powers of α_n, one can obtain a simple closed form for the ring diagrams given by

$$-\beta\left[\sum_{n\neq 0}\frac{1}{2}\frac{\alpha_n^2}{1+\beta\langle\Delta V^{(2)}\rangle_\alpha\alpha_n^2}\ \partial^2\right]\Delta V=-\beta\mathscr{D}\Delta V, \tag{3.19}$$

where $\mathscr{D}$ should be understood as an operator. Furthermore, one can include diagrams with multiple rings hanging on the same vertex which leads symbolically to

$$=-\beta\left(1+\mathscr{D}+\frac{1}{2}\mathscr{D}+\frac{1}{2^2 2!}\mathscr{D}^2+\cdots\right)\Delta V. \tag{3.20}$$

Equation (3.20) now defines an effective potential which has the same form as Eq. (3.13), except the Gaussian width factor is now given by

$$\bar{\alpha}=\sum_{n\neq 0}\frac{\alpha_n}{1+\beta\langle\Delta V^{(2)}\rangle_\alpha\alpha_n}. \tag{3.21}$$

This is a particularly useful form of the equation for the effective potential because it involves only the second derivative of the potential averaged about the centroid using the unoptimized reference propagator width factor α.

As has already been suggested, ΔV in Eq. (3.21) can be replaced by an effective potential difference $\Delta\bar{V}$. The procedure here is called the renormalization. Analytically, the renormalized element appears as an unknown variable to be solved from self-consistent equations which relate the given unrenormalized quantities to the renormalized ones. Usually, it is straightforward to discover such a relationship by observing the topology of diagrams. As a result of the renormalization of the vertices, one arrives at the expression for the renormalized potential difference $\Delta\bar{V}$ by replacing the Gaussian width factor α in the averaging in the right-hand side of Eq. (3.21) by the effective width factor $\bar{\alpha}$. Note that this equation must now be solved self-consistently. The resulting expression for $\Delta\bar{V}$ is given by

$$\Delta\bar{V}=\langle\Delta V(q_c+\tilde{q})\rangle_{\bar{\alpha}} \tag{3.22}$$

with

$$-\beta\Delta\bar{V}\equiv \tag{3.23}$$

and $\langle\cdots\rangle_{\bar{\alpha}}$ denotes a Gaussian average with a width factor

$$\bar{\alpha}=\sum_{n\neq 0}\frac{\alpha_n}{1+\beta\Delta\bar{V}^{(2)}\alpha_n}. \tag{3.24}$$

The notation "$\Delta\bar{V}^{(2)}$" means that the second derivative of $\Delta V(q_c+\tilde{q})$ is taken with respect to $\tilde{q}$. Renormalized quantities will be denoted hereafter with an overbar. Diagrammatically, a black vertex stands for a renormalized potential [cf. Eq. (3.23)], while a bold line stands for a renormalized centroid-constrained propagator. Again, the underlying logic of renormalization is not new and has been used many times in, e.g., Green's function theory, mean field theory, etc. To our knowledge, it has not been applied in a general way to treat the centroid density. A multidimensional generalization is discussed in the Appendix.

The seemingly complicated equations given above actually have a relatively simple interpretation. By substituting the centroid-constrained propagator for the LHO into Eq. (3.24), and using a general LHO frequency ω such that $\Delta V(q_c+\tilde{q})=V(q_c+\tilde{q})-\frac{1}{2}m\omega^2\tilde{q}^2$ and $\alpha_n^{-1}=m\beta(\Omega_n^2+\omega^2)$, the renormalized LHO frequency $\bar{\omega}$ can be specified from the definition

$$m\bar{\omega}^2\equiv\langle V^{(2)}(q_c+\tilde{q})\rangle_{\bar{\alpha}} \tag{3.25}$$

The value of the renormalized LHO frequency is determined from the solution to the above transcendental equation, where the renormalized Gaussian width factor in Eqs. (3.24) and (3.25) is now given by

$$\tilde{\alpha}=\sum_{n\neq 0}\frac{1}{m\beta(\Omega_n^2+\tilde{\omega}^2)}. \tag{3.26}$$

It should be noted that these equations are to be solved for each position of the centroid q_c. The frequency in Eq. (3.25) is exactly the effective frequency obtained for the optimized LHO reference system using the path integral centroid density version of the Gibbs–Bogoliubov variational method.[8] Originally suggested by Feynman[8,9] as an approximate route to the quantum partition function, this variational theory has also been employed in the evaluation of quantum rate constants[12(a)] and to improve the convergence of path integral Monte Carlo simulations.[10] The present derivation, however, does not depend on a specific reference system as long as it is quadratic. In addition, Eqs. (3.25) and (3.26) are not derived from any variational principle, but are instead the result of diagram renormalization. More importantly, the diagrammatic analysis provides a way to systematically improve on the variational theory.

In order to improve on the optimized LHO theory for the effective centroid potential, one needs to consider the contribution from higher order diagrams. One way to accomplish this is to diagrammatically impose the condition $\langle\Delta V^{(2)}\rangle_{\tilde{\alpha}}=0$ [cf. Eqs. (3.25) and (3.26)]. This condition specifies that all vertices linked to two lines will vanish, i.e.,

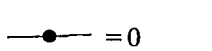 $=0$ (3.27)

Consequently, all diagrams containing this element will vanish, giving the result $\alpha=\tilde{\alpha}$. The leading corrections in the centroid density expansion in Eq. (3.10) are then given by

 $=\frac{1}{2!3!}\beta\langle\Delta V^{(3)}\rangle_{\tilde{\alpha}}^2\frac{1}{\hbar}\int_0^{\hbar\beta}d\tau\,\alpha^3(\tau)$ (3.28)

and

 $=\frac{1}{2!4!}\beta\langle\Delta V^{(4)}\rangle_{\tilde{\alpha}}^2\frac{1}{\hbar}\int_0^{\hbar\beta}d\tau\,\alpha^4(\tau)$ (3.29)

where the centroid-constrained propagator for the LHO is given by

$$\tilde{\alpha}(\tau)=\frac{1}{m\beta\tilde{\omega}^2}\left[\frac{b/2}{\sinh(b/2)}\cosh(1-2u)b/2-1\right], \tag{3.30}$$

in which $b=\hbar\beta\tilde{\omega}$ and $u=\tau/\hbar\beta$. These two terms provide an improvement on the optimized harmonic reference centroid density approximation, giving

$$\rho_c=\rho_{c,\mathrm{ref}}\exp\left\{-\beta\left[\langle\Delta V\rangle_{\tilde{\alpha}}-\frac{1}{2!3!}\frac{f_3(b)}{\hbar\tilde{\omega}}\left(\frac{\hbar}{m\tilde{\omega}}\right)^3\langle\Delta V^{(3)}\rangle_{\tilde{\alpha}}^2-\frac{1}{2!4!}\frac{f_4(b)}{\hbar\tilde{\omega}}\left(\frac{\hbar}{m\tilde{\omega}}\right)^4\langle\Delta V^{(4)}\rangle_{\tilde{\alpha}}^2+\cdots\right]\right\}. \tag{3.31}$$

Here, $f_n(b)$ is a dimensionless coefficient defined by

$$f_n(b)=\left(\frac{1}{b}\right)^{n-1}\int_0^1 du\left[\frac{b/2}{\sinh(b/2)}\cosh(1-2u)b/2-1\right]^n, \tag{3.32}$$

which becomes a constant in the limit of large b. More corrections can be included by adding more diagrams. This procedure will be discussed in the next subsection in the context of renormalization of the centroid-constrained propagator (i.e., the lines).

C. Renormalization of the lines

The other essential element of the diagrams is the line which represents the centroid-constrained propagator. The renormalization of vertices leads to the evaluation of the effective potential while the renormalization of lines leads to the evaluation of the Euclidean centroid-constrained propagator defined in Eq. (2.1). This propagator can be obtained formally from Eq. (2.5) combined with Eq. (3.9).

Following the diagrammatic analysis of Sec. II, all the leading diagrams for $C_c(\tau,q_c)$ are obtained from Eq. (3.10), i.e.,

$C_c(\tau,q_c)=$ 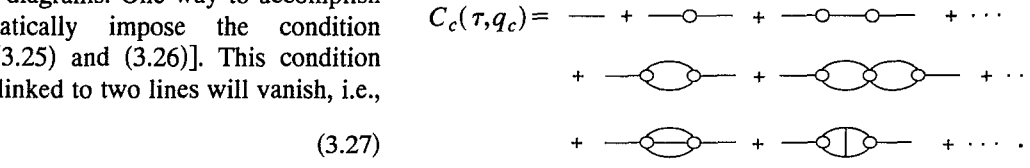 (3.33)

Obviously, the above collection of diagrams represents all possible contributions to the centroid-constrained correlation function. In fact, all the decorations attached to the intermediate vertices can be removed if the vertex is renormalized. This operation can be achieved by replacing all the ΔV's by $\Delta\tilde{V}$'s, giving

$$\Delta\tilde{V}=\langle\Delta V(q_c+\tilde{q})\rangle_{C_c(0,q_c)}, \tag{3.34}$$

where the Gaussian width factor is now $C_c(0,q_c)$ instead of $\alpha(0)$. In the case of fully renormalized vertices, $C_c(0,q_c)$ is equivalent to the renormalized reference centroid-constrained propagator $\tilde{\alpha}$ of Eq. (3.24). These two notations will not be distinguished hereafter.

The simplest set of lines is the chain collection, given by

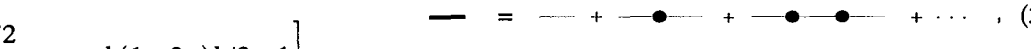 (3.35)

where the bold line stands for a renormalized line. This diagram can also be expressed in the compact form

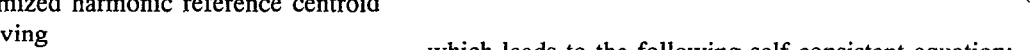 (3.36)

which leads to the following self-consistent equation:

$$\tilde{\alpha}_n=\alpha_n-\beta\Delta\tilde{V}^{(2)}\tilde{\alpha}_n\alpha_n. \tag{3.37}$$

By noting that $\tilde{\alpha}=\Sigma_{n\neq 0}\tilde{\alpha}_n$, it is seen that Eqs. (3.34) and (3.37) are the same as the optimized LHO reference equations in Eqs. (3.22) and (3.24) derived in the last section. In fact, differentiating a ring collection of the generating functional always produces a chain collection in the correlation

diagrams.[16] The multidimensional generalization of the above equation is described in the Appendix.

The next stage in the analysis is to include all the two-line-loop corrections in the renormalization given by

$$=\tfrac{1}{2}\,\alpha_n\bar{\alpha}_n\overline{\alpha_n^2}(\beta\Delta\bar{V}^{(3)})^2-\tfrac{1}{4}\,\alpha_n\bar{\alpha}_n(\overline{\alpha_n^2})^2(\beta\Delta\bar{V}^{(3)})^2\beta\Delta\bar{V}^{(4)}+\cdots . \tag{3.38}$$

Because of the imaginary time convolutions in the expression, the analytical expressions for the above diagrams are written in Fourier space, where $\overline{\alpha_n^2}$ is the contribution from the two-line loop given by

$$\overline{\alpha_n^2}=\sum_{m\neq 0}\bar{\alpha}_{n-m}\bar{\alpha}_m . \tag{3.39}$$

Since $\overline{\alpha^2}$ is a convolution expression, the self-consistent equation for $\bar{\alpha}$ is not local in Fourier space and therefore we can no longer seek a single effective frequency solution as in Eq. (2.15). As a matter of fact, this analysis shows that the optimized LHO reference system reaches the maximum capacity for a quadratic potential to approximate an anharmonic potential and any further corrections are beyond an effective frequency description.

The infinite summation in Eq. (4.10) can be carried out to yield a closed equation given by

$$\bar{\alpha}_n=\alpha_n-\alpha_n\bar{\alpha}_n\beta\Delta\bar{V}^{(2)}+\frac{(1/2)\alpha_n\bar{\alpha}_n\overline{\alpha_n^2}(\beta\Delta\bar{V}^{(3)})^2}{1+(1/2)\overline{\alpha_n^2}(\beta\Delta\bar{V}^{(4)})}, \tag{3.40}$$

which can be solved numerically. It is important to incorporate infinite terms corresponding to the same class of diagrams, so that at low temperature and high aharmonicity, the self-consistent equation will not diverge.

Further corrections to the propagator diagrams will consist of multiline loops and their combinations. However, the expressions become increasingly complicated and we have not been able to reach a general result for the infinite summation of all the multiline loops. Apart from the simple multiline loops, there also exist a large number of irreducible diagrams that are not included in the above renormalization scheme. It may be possible that information from some of the lower-order diagrams could help in the construction of an accurate renormalization equation by means of a Padé approximant or a continued fraction scheme.

As shown in Sec. II, the centroid-constrained Euclidean correlation function is of central importance in studying equilibrium properties via the centroid density perspective. Even more importantly, its real-time counterpart is essential in describing the quantum dynamics of a system (cf. the companion paper[13] and Ref. 14). The real time and imaginary time correlation functions are of course related by the analytical continuation $\tau\rightarrow it$, so the detailed study of the Euclidean centroid-constrained correlation function presented in this section helps us to understand the real time behavior of quantum systems.

TABLE I. The average value $\langle q^2\rangle$ for the potential in Eq. (4.1) evaluated with the centroid-based formalism in Eq. (2.18) and with various levels of approximation for the centroid density.[a] The exact results were obtained by path integral Monte Carlo.

β	$\langle q^2\rangle_{\text{exact}}$	$\langle q^2\rangle_1$	$\langle q^2\rangle_2$	δ_1	δ_2
5	1.378	1.361	1.371	1.3	0.5
7	1.382	1.352	1.372	2.2	0.7
9	1.384	1.344	1.372	2.9	0.9

[a]The results $\langle q^2\rangle_1$ are based on the optimized LHO reference potential approximation for the centroid density in Eqs. (3.22)–(3.26), while $\langle q^2\rangle_2$ are the results including the higher-order corrections (3.28) and (3.29). The quantities δ_1 and δ_2 are the percentage errors of $\langle q^2\rangle_1$ and $\langle q^2\rangle_2$, respectively, compared with the numerically exact result.

IV. APPLICATIONS

In this section, the results of calculations which probe the accuracy of the four main topics discussed in this paper are presented. These topics are: (1) the centroid-based formulation for calculating equilibrium averages (Sec. II B); (2) the centroid-based formulation for calculating imaginary time correlation functions (Sec. II C); (3) the analytic diagrammatic approach for the calculation of the centroid density (Sec. III B); and (4) the analytic diagrammatic approach for calculating the imaginary time propagator (Secs. II A) and III C).

For all of the above, the numerical calculations are based on a completely nonquadratic potential given by

$$V(q)=q^3+q^4/2, \tag{4.1}$$

where the mass m and $\hbar$ are taken to be unity. The inverse temperature β is thus the same as the value as the dimensionless parameter $\beta\hbar\omega$. All of the analytical results on this application are compared with PIMC simulation results. To achieve good convergence, the path integral simulations employed $P=100$ discretizations (or "polymer" quasiparticles)

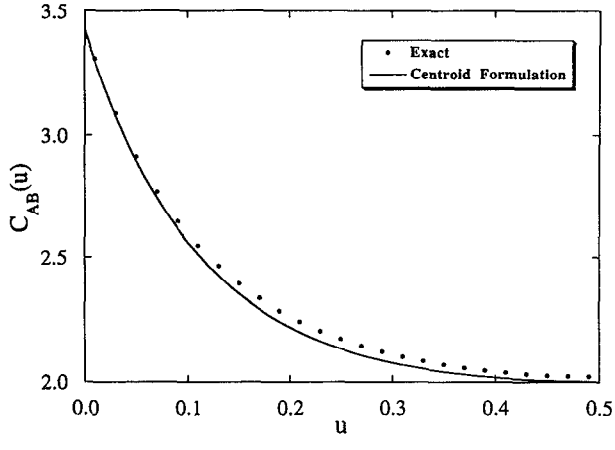

FIG. 4. A plot of the imaginary time correlation function $\langle q^2(\tau)q^2(0)\rangle$ for the nonquadratic potential described in Sec. IV [Eq. (4.1)]. The correlation function is plotted as a function of the dimensionless variable $u=\tau/\hbar\beta$ with $\beta=5$. The solid circles show the numerically exact results, while the solid line is for the optimized LHO theory in Eqs. (3.22)–(3.26) with the centroid-based formulation of the correlation function in Eq. (2.18).

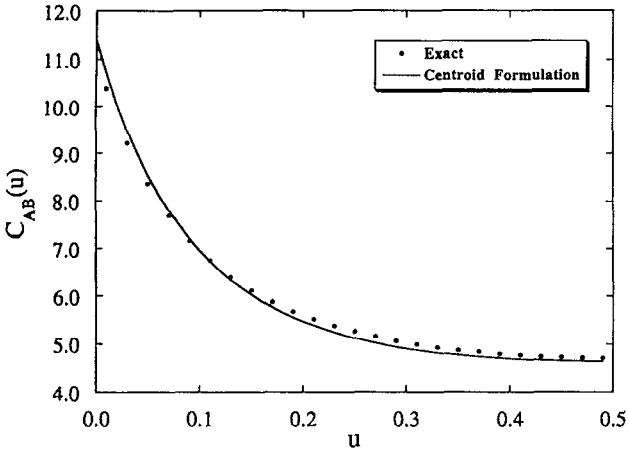

FIG. 5. A plot of the imaginary time correlation function $\langle q^3(\tau)q^3(0)\rangle$ for the nonquadratic potential described in Sec. IV [Eq. (4.1)]. The correlation function is plotted as a function of the dimensionless variable $u=\tau/\hbar\beta$ with $\beta=5$. The solid circles show the numerically exact results, while the solid line is for the optimized LHO theory in Eqs. (3.22)–(3.26) with the centroid-based formulation of the correlation function in Eq. (2.18).

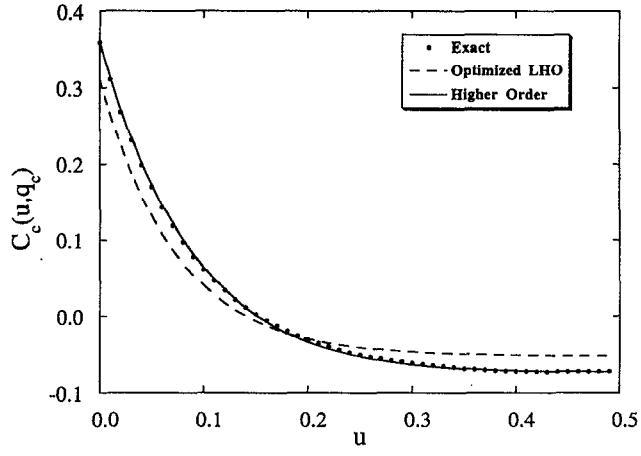

FIG. 6. A plot of the centroid-constrained correlation function $C_c(\tau,q_c)$ defined in Eq. (2.1) for the nonquadratic potential described in Sec. IV [Eq. (4.1)] The numerically exact results are shown by the solid circles. The correlation function obtained from the optimized LHO approximation in Eq. (3.37) is shown by the dashed line, while the solid line shows the results obtained by including the two-line-loop correction from Eq. (3.40). The correlation functions are plotted as a function of $u=\tau/\hbar\beta$ and for $\beta=10$ and $q_c=0.0$.

and 10^6 MC passes. The number of beads moved on each trial was adjusted to yield an acceptance rate of 50%.

In Table I, the values for the equilibrium average $\langle q^2\rangle$ are tabulated for the potential in Eq. (4.1) as calculated by PIMC and by the centroid formulation in Eq. (2.10) with the optimized LHO approximation to the centroid density [cf. Eqs. (3.22)–(3.26)]. Also tabulated are the analytic results obtained using the optimized LHO theory with the higher-order corrections in Eqs. (3.28) and (3.29). The results are shown for various temperatures. Clearly, the centroid approach is an accurate one. It should also be noted that these calculations represent a stringent test of the centroid formulation because the potential in Eq. (4.1) contains no intrinsic quadratic term. One consequence of this is that the optimized LHO approximation for $\langle q^2\rangle$ actually gets progressively worse as the temperature is lowered, reflecting the essential nonquadratic character of the ground state.

In Fig. 4, the imaginary time correlation function $\langle q^2(\tau)q^2(0)\rangle$ is plotted for a temperature of $\beta=5$ and as a function of the dimensionless variable $u=\tau/\hbar\beta$. The solid circles depict the exact PIMC result, while the solid line is for the optimized LHO result along with the centroid-based formulation of the correlation function in Eq. (2.18). In Fig. 5, similar results are shown for the correlation function $\langle q^3(\tau)q^3(0)\rangle$. Again, the centroid-based formalism is in very good agreement with the numerically exact result.

Although the calculations described above provide an indirect test of the analytic expressions derived for the centroid density, it is desirable to provide a direct test. Therefore, the quantum correction factor for a Eckart barrier has been calculated and tabulated in Table II within the context of path integral quantum transition state theory.[12] In the context of that theory, the quantum correction factor Γ to the classical rate constant is given by

$$\Gamma=\rho_c(q^*)/\rho_{\rm cl}(q^*), \tag{4.2}$$

where ρ_c and $\rho_{\rm cl}$ are the centroid density and the classical density at the barrier top ($q=q^*$), respectively. Since the centroid density is larger than the classical density at the barrier top, the quantum rate is enhanced by the correction factor Γ. In their paper, Voth *et al.*[12(a)] evaluated this factor for an Eckart barrier at different temperatures and found the difference between the numerical path integral results and the optimized LHO approximation for the centroid density increases as the temperature is lowered. Therefore, the higher-order analytic corrections in Eq. (3.31) become important in the extreme quantum limit. As the Eckart barrier is an even potential, the cubic term in Eq. (3.31) vanishes at the barrier top and the leading correction is quartic. In Table II, the results are listed from the optimized LHO reference approximation, from the optimized LHO approximation including the higher order corrections, and from the PIMC results. For the last two entries, the quartic correction seems to

TABLE II. Quantum correction factors[a] from Eq. (4.2) for the Eckart barrier.[b]

u	Γ_1	Γ_2	$\Gamma_{\rm MC}$
6	4.4	4.4	4.4
8	15.0	17.0	17.0
10	73.0	110.6	105.0
12	514.0	1278.0	1240.0

[a]The quantum corrections Γ_1 are based on the optimized LHO reference potential approximation for the centroid density in Eqs. (3.22)–(3.26), while Γ_2 are the results including the higher-order terms in Eqs. (3.31). The quantum correction $\Gamma_{\rm MC}$ is the path integral Monte Carlo result reported in Ref. 12(a).

[b]The Eckart barrier potential is given by $V(q)=V_0\,\mathrm{sech}^2(q/a_0)$ with the parameter values $2\pi V_0/\hbar\omega_b=12.0$ and $u=\beta\hbar\omega_b$ in the present calculations, and ω_b is the magnitude of the classical barrier frequency.

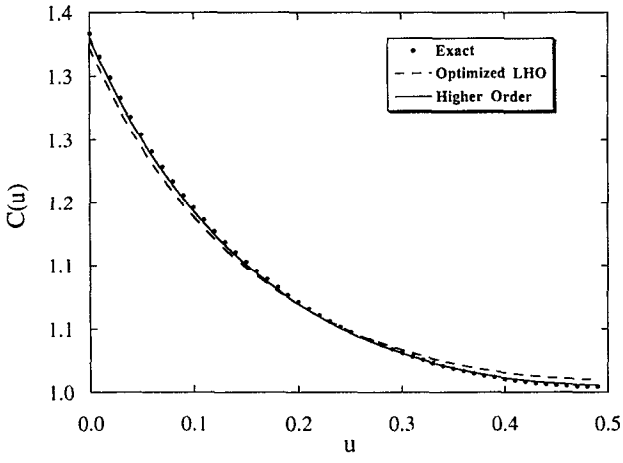

FIG. 7. A plot of the imaginary time position correlation function $C(\tau)$ in Eq. (2.3) for the nonquadratic potential described in Sec. IV [Eq. (4.1)]. The numerically exact results are shown by the solid circles. The correlation function obtained using the centroid-constrained optimized LHO approximation in Eq. (3.37) is shown by the dashed line, while the solid line shows the results obtained by including the two-line-loop correction from Eq. (3.40). In the two latter cases, the correlation function $C(\tau)$ was obtained by averaging the appropriate analytical centroid-constrained correlation function over the numerically determined centroid density. The results are plotted as a function of $u=\tau/\hbar\beta$ and for $\beta=5$.

slightly overestimate the PIMC result, although in either case, the analytic theory is essentially exact to within the MC error (~5%) of the numerical results.

A final set of calculations was designed to test the accuracy of the analytic expressions for the centroid-constrained correlation function $C_c(\tau,q_c)$ [Eq. (2.1)], as well as the imaginary time position correlation function $C(\tau)$ obtained by averaging the centroid-constrained propagator over the coordinate space weighted by the centroid density. To demonstrate the effect of the higher-order correction terms in Eq. (3.40), the centroid-constrained propagator was first evaluated using the optimized LHO approximation in Eq. (3.37) as shown by the dashed line in Fig. 6 for $\beta=10$ and $q_c=0$. The result obtained by including the two-line-loop correction in Eq. (3.40) is shown by the solid line, while the PIMC results are given by the solid circles. The results are again calculated as a function of $u=\tau/\hbar\beta$. Though the effective LHO approximation provides a good approximation to the exact centroid-constrained correlation function, the correction from the two-line-loop diagram renormalization clearly improves the agreement with the numerical data. In fact, the latter theoretical prediction virtually coincides with the exact PIMC result.

Figure 7 shows the imaginary time position correlation function $C(\tau)$ for $\beta=5$. The effective frequency $\bar{\omega}$ was solved self-consistently from Eqs. (3.25) and (3.26) at each centroid position q_c and then the centroid-contrained optimized LHO correlation function was averaged with the numerical centroid density. As seen from Fig. 7, good agreement was obtained with the numerical result. Even better agreement was obtained from Eq. (3.40) using the two-line-loop correction (solid curve). Again, the deviation from the exact result in either case is quite small.

V. CONCLUDING REMARKS

In the present paper, the basic computational procedures of equilibrium statistical mechanics have been reformulated in order to cast the path integral centroid density into a role of the underlying statistical distribution in quantum statistical mechanics. The usual expressions for equilibrium averages and imaginary time correlation functions have been modified so that the final answer is obtained by averaging an effective centroid-dependent function over the centroid distribution. These effective functions involve, in the case of an operator average, a quasiclassical centroid-dependent function, or, in the case of an imaginary time correlation function, a quasiclassical operator product. In each case, the quasiclassical centroid-dependent quantity is formulated as a Gaussian averaged function "broadened" by the intrinsic quantum thermal width of the particle.

In addition to the computational formalism for averages and correlation function, a formally exact diagrammatic perturbation theory for the centroid density and related quantities has been formulated and analyzed in some detail. The connection between different levels of diagrammatic summation and renormalization in the perturbation theory and the Feynman–Hibbs[7] or variational theories[9–11] for the centroid density have been identified, leading to a systematic analytic methodology for improving upon the latter two approaches. Correspondingly, specific correction factors have been derived and excellent agreement with numerical calculations obtained.

The primary motivation for the development of the present formalism arises from the numerous appealing properties of the centroid density such as its compelling analogy[7] with the classical Boltzmann density and the topological simplicity of its underlying diagrammatic representation. Another motivation is the apparently central role occupied by the centroid density in the path integral quantum transition state theory[12] for activated rate constants. These facts have led us to develop the more general perspective presented in the present paper. The companion paper[13] explores the intriguing role played by the centroid variable and centroid density in dynamical quantum time correlation functions.[14] Applications of the centroid-based formalism described in the present and companion papers will be the subject of future research.

ACKNOWLEDGMENTS

This research was supported by the National Science Foundation and the Office of Naval Research. GAV is a recipient of a National Science Foundation Presidential Young Investigator Award, a David and Lucile Packard Fellowship in Science and Engineering, an Alfred P. Sloan Foundation Research Fellowship, and a Dreyfus Foundation New Faculty Award.

APPENDIX: THE RENORMALIZED CENTROID-CONSTRAINED PROPAGATOR IN MULTIDIMENSIONAL SPACE

It is first assumed that the reference centroid-constrained propagator [cf. Eq. (3.2)] for a multidimensional system is a

diagonal matrix, i.e., $A(\tau)=\delta_{\mu,\nu}\alpha_\nu(\tau)$, where the upper case letters here stand for matrices or vectors. Because there are mixed-index partial derivatives at the vertices, the multidimensional centroid-constrained propagator $C_c(\tau,q_c)$ matrix [cf. Eq. (2.1)] is not necessarily diagonal. (Note here that q_c is now the *multidimensional* centroid variable.) The first correction to consider is the chain summation in Eq. (3.36), which gives rise to the optimized centroid-constrained correlation function matrix

$$C_c(\tau,q_c)=A-\beta\langle(AD):(DC_c)\Delta V\rangle_{C_c}, \tag{A1}$$

where D is the partial derivative vector $D_\mu=\partial_\mu$ and ΔV is the scalar multidimensional potential difference. The notation $\langle\cdots\rangle_{C_c}$ here denotes a multidimensional Gaussian average with width factors taken from the matrix of optimized $C_c(0,q_c)$ values. Upon substituting the explicit form of A in Eq. (A1), one obtains the multidimensional matrix analog of Eq. (3.37) as

$$C_{c,n}=\frac{1}{m\beta\Omega_n^2+\beta\langle(D:D)\Delta V\rangle_{C_c}}, \tag{A2}$$

which leads to the definition of the optimized frequency tensor

$$m\tilde{\omega}^2_{\mu,\nu}=\langle\partial_\mu\partial_\nu V\rangle_{C_c}. \tag{A3}$$

This is the same self-consistent equation obtained previously [see, e.g., Eq. (2.48) of Ref. 10]. The two-line-loop correction in Eq. (3.38) is more complicated, but as long as one uses the tensor prescription, it is always possible to generalize the one-dimensional equations to multidimensional space.

[1] R. P. Feynman and A. R. Hibbs, *Quantum Mechanics and Path Integrals* (McGraw–Hill, New York, 1965).

[2] R. P. Feynman, *Statistical Mechanics* (Addison–Wesley, Reading, MA, 1972), Chap. 3.

[3] For reviews of path integral methods, both numerical and analytical, see B. J. Berne and D. Thirumalai, Annu. Rev. Phys. Chem. **37**, 401 (1986); D. L. Freeman and J. D. Doll, Adv. Chem. Phys. **70**, 139 (1988); J. D. Doll and D. L. Freeman, *ibid.* **73**, 289 (1989); *Quantum Simulations of Condensed Matter Phenomena*, edited by J. D. Doll and J. E. Gubernatis (World Scientific, Singapore, 1990); D. Chandler, in *Liquides, Cristallisation et Transition Vitreuse, Les Houches, Session LI*, edited by D. Levesque, J. P. Hansen, and J. Zinn-Justin (Elsevier, New York, 1991).

[4] D. Chandler and P. G. Wolynes, J. Chem. Phys. **74**, 4078 (1981); D. Chandler, J. Phys. Chem. **88**, 3400 (1984).

[5] See, e.g., Ref. 2, Chap. 8.

[6] See, e.g., the analytical description of an electron in water in D. Laria, D. Wu, and D. Chandler, J. Chem. Phys. **95**, 4444 (1991); for numerical path integral studies of the hydrated electron, see A. Wallqvist, D. Thirumalai, and B. J. Berne, *ibid.* **86**, 6404 (1987); J. Schnitker and P. J. Rossky, *ibid.* **86**, 3471 (1987); R. N. Barnett, U. Landman, C. L. Cleveland, and J. Jortner, *ibid.* **88**, 4421 (1988).

[7] See, e.g., Ref. 1, pp. 279–286.

[8] See, e.g., Ref. 1, pp. 303–307 and Ref. 2, pp. 86–96.

[9] R. P. Feynman and H. Kleinert, Phys. Rev. A **34**, 5080 (1986); R. Giachetti and V. Tognetti, Phys. Rev. Lett. **55**, 912 (1985); Phys. Rev. B **33**, 7647 (1986); W. Janke and H. Kleinert, Chem. Phys. Lett. **137**, 162 (1987); see also Ref. 12(a).

[10] J. Cao and B. J. Berne, J. Chem. Phys. **92**, 162 (1987).

[11] G. A. Voth, Phys. Rev. A **44**, 5302 (1991).

[12] (a) G. A. Voth, D. Chandler, and W. H. Miller, J. Chem. Phys. **91**, 7749 (1989); (b) G. A. Voth, Chem. Phys. Lett. **170**, 289 (1990); for a review of path integral quantum transition state theory, see G. A. Voth, J. Phys. Chem. **97**, 8365 (1993); (c) see also the related work of M. J. Gillan, J. Phys. C **20**, 3621 (1987).

[13] J. Cao and G. A. Voth, J. Chem. Phys. **100**, 5106 (1994).

[14] J. Cao and G. A. Voth, J. Chem. Phys. **99**, 10070 (1993).

[15] See, e.g., M. S. Swanson, *Path Integrals and Quantum Processes* (Academic, San Diego, 1992), Sec. 4.2.

[16] T. Morita and K. Hiroike, Prog. Theor. Phys. **25**, 537 (1961); C. De Dominicis, J. Math. Phys. **3**, 183 (1962).

[17] J. E. Mayer, J. Chem. Phys. **10**, 629 (1942).

[18] See, e.g., Ref. 2, pp. 192–197; R. D. Mattuck, *A Guide to Feynman Diagrams in the Many-Body Problem*, 2nd ed. (McGraw–Hill, New York, 1976).

[19] A. L. Fetter and J. D. Walecka, *Quantum Theory of Many-Particle Systems* (McGraw–Hill, New York, 1971); E. N. Economou, *Green's Functions in Quantum Physics* (Springer, Berlin, 1983).